Dalton Transactions

ROYAL SOCIETY OF CHEMISTRY

PAPER

Published on 11 June 2026
Licence and permissions

Check for updates

Cite this: *Dalton Trans.*, 2026, **55**, 9767

Organotin(IV) compounds with potent cytotoxicity, DNA damage, cell cycle arrest, and pro-apoptotic effects

Shubham Sharma,[a] Margrét H. Ögmundsdóttir,[b] Helga M. Ögmundsdóttir,[b] Snorri Th. Sigurdsson[a] and Krishna K. Damodaran*[a]

Received 8th April 2026,
Accepted 10th June 2026

DOI: 10.1039/d6dt00812g

rsc.li/dalton

Platinum-based anticancer agents exert their activity through DNA cross-linking but are limited by systemic toxicity, poor selectivity, and the emergence of drug resistance, underscoring the need for alternative mechanisms of action. We have selected organotin(IV) center with intrinsic cytotoxic potential and combined it with multifunctional ligands containing functional moieties that could enhance the anticancer efficacy, and synthesised two organotin(IV) complexes, Bu_2SnL and Ph_2SnL (L = benzyl 2-(diphenylphosphoryl)hydrazine-1-carbodithioate), to explore a non-cross-linking DNA-damaging strategy. Cellular uptake studies revealed substantial intracellular accumulation of both complexes, with preferential nuclear localization. *In vitro* cytotoxicity assays demonstrated potent antiproliferative activity against breast cancer T-47D cells, with Bu_2SnL exhibiting an IC_{50} value of 0.32 ± 0.04 μM, representing an ≈88-fold increase in potency relative to cisplatin. Mechanistic investigations indicated that these complexes induce pronounced DNA damage, G1-phase cell cycle arrest, and intracellular ATP depletion, ultimately leading to apoptotic cell death. The DNA interaction studies suggest the possibility of a distinct binding mode compared to cisplatin, and we propose that the complex is coordinating to phosphate groups rather than nucleobase cross-linking. These findings indicate that organotin(IV) complexes are promising anticancer candidates that may offer a different mechanism of action, potentially overcoming the limitations of cisplatin.

Introduction

Cancer remains one of the leading causes of mortality globally, contributing to approximately 9.7 million deaths in 2022.[1] According to estimates from the World Health Organization (WHO), approximately 20 million new cancer cases were reported globally in 2022 and this number is projected to rise significantly, reaching 35 million cases by 2050.[1] Chemotherapy remains the most effective option compared to other methods, where the administration of the anticancer drugs inhibit the uncontrolled growth of cancer cells.[2] Metal complexes-based anticancer drugs have several advantages over conventional organic small-molecule drugs, due to their unique physicochemical properties, such as charge variation, diverse structural and bonding configurations, metal–ligand interactions, and redox activity *etc*.[3] Since the discovery and FDA approval of cisplatin ($[Pt(NH_3)_2Cl_2]$) for cancer treatment, there has been growing interest in the use of metal-based compounds within the biomedical field.[4,5] Despite the significant clinical success of cisplatin, carboplatin, and oxaliplatin,[6–8] they have severe side effects, a limited spectrum of activity, and, more concerningly, a rising incidence of drug-resistant tumours, which restricts the broader clinical application of these compounds.[9–12] This prompted researchers to explore other metal complexes, including ruthenium, palladium, iridium, gold, rhodium, and tin complexes,[13,14] which showed promising results in preclinical studies.[3,15–18] We have selected tin(IV) complexes owing to their unique structural properties and distinct mechanisms of action compared to platinum-based drugs.[19]

Organotin complexes are known for their exceptional target specificity, reduced systemic toxicity, broad-spectrum antitumor activity, and non-cross resistance, making them a novel class of promising antitumor agents with excellent therapeutic potential.[20–22] The organic ligands also play a crucial role in the cytotoxic potential, lipophilicity, stability, aqueous solubility, and target-binding affinity of anticancer agents.[23] Organotin moiety largely contributes to the cytotoxic effects, and the organic ligands play a critical role in modulating

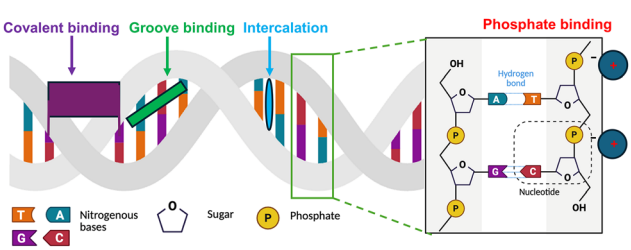
[a]*Department of Chemistry, Science Institute, University of Iceland, 107, Iceland. E-mail: krishna@hi.is; Fax: +354552 8911; Tel: +354 525 4846*
[b]*Biomedical Center, Faculty of Medicine, University of Iceland, Sturlugata 8, 102 Reykjavik, Iceland*

This journal is © The Royal Society of Chemistry 2026

activity, biodistribution, and stability.[19,22–24] Organotin(IV) complexes featuring ligands with bioactive functional groups display excellent anticancer activities,[19,25,26] and the functional moieties could contribute to the biological activity of the organometallic complex and influences its ADME properties.[27]

The synthesis of organotin(IV) complexes based on multifunctional ligands by incorporating various functional groups is challenging, and their anticancer potential remains largely underexplored.[24] The anticancer activities of glutamine-conjugated organotin(IV) Schiff base complexes suggest that the presence of glutamine contributes to increased tumour selectivity and improved antiproliferative effects.[22] We reported the anticancer activities of organotin(IV) complexes with multifunctional groups and showed that the complexes were more effective than cisplatin against different cancer cell lines.[28] The mode of action of the organotin(IV) complexes was different compared to platinum-based drugs,[19] specifically DNA binding. DNA continues to be a critical target in anticancer therapy because cancer cells rely on constant DNA replication and repair to support rapid proliferation, making them highly vulnerable to compounds that induce DNA damage or disrupt DNA-related pathways *via* intercalation, major/minor groove binding, covalent binding, and electrostatic interaction, *etc*. (Scheme 1).[29,30]

The mechanism of action of cisplatin and related platinum-based drugs involves covalent binding to DNA bases, primarily guanine, resulting in intrastrand and interstrand cross-links that impede DNA replication and transcription.[31] Efforts have been made to identify different binding modes, and Komeda *et al.* reported an alternative DNA-binding mode for organometallic complexes, referred to as a phosphate clamp that targets the phosphate groups of the DNA backbone.[32] The DNA adducts formed by these binding modes are distinct from those formed at nucleobases, which could overcome the clinical resistance towards platinum-based drugs.[32] Organometallic complexes interact with the negatively charged phosphate groups of the DNA backbone.[33–36] Interestingly, organotin(IV) moiety displays a strong affinity for these phosphate backbones,[37] but this mode of DNA binding remains largely unexplored for organotin(IV) complexes. In this work, we report the synthesis, chemical characterisation, stability, and biological evaluation of two tin(IV) complexes based on multifunctional ligands containing phosphorus (phosphine oxide), sulphur (dithioformate), and nitrogen (hydrazine) moieties.



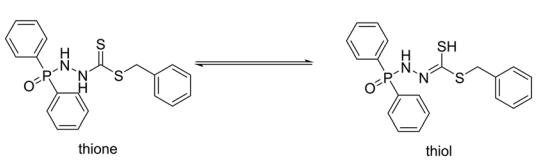
Scheme 1 Representation of various Drug-DNA binding modes.

Results and discussion

The combination of multifunctional groups within a single ligand is a promising strategy to enhance anticancer activity through synergistic effects, compared to a single component.[38] We have demonstrated that incorporating functional groups such as phosphine oxide and dithio moieties into organometallic tin(IV) compounds yield anticancer agents with greater efficacy than cisplatin.[28] The phosphorus moieties might play a critical role; for example, by enhancing aqueous solubility in prodrug design or facilitating chemical transformations that generate the active drug species.[39,40] Sulphur-containing molecules have long been employed as chemoprotective agents.[41–44] Organotin(IV) dithiocarbamate complexes have been reported to exhibit enhanced cytotoxicity in cancer cell lines due to synergistic effects between the organotin center and the dithiocarbamate ligand.[20] In this work, we have designed a multifunctional ligand, benzyl 2-(diphenylphosphoryl)hydrazine-1-carbodithioate (**L**) based on phosphine oxide and dithio moieties with an additional functional group, namely, hydrazine moiety. Over 400 hydrazine-related compounds have been tested for their potential to kill cancer cells, and even the simplest design, hydrazine sulphate, has been investigated as an anticancer treatment for more than 30 years.[45,46]

Synthesis and characterisation of complexes

The multifunctional ligand (**L**) was synthesised by reacting benzyl hydrazinecarbodithioate (**PL**) and phosphinic chloride (Schemes S1 and S2, see SI). The precursor **PL** was synthesised by reacting benzyl bromide and potassium hydrazinecarbodithioate[47] in a methanol–water mixture (Scheme S1, see SI).[48] This intermediate was then subjected to a substitution reaction with diphenyl phosphinic chloride in the presence of triethylamine, leading to the desired ligand scaffold, benzyl 2-(diphenylphosphoryl)hydrazine-1-carbodithioate (**H_2L**). Compounds **PL** and **H_2L** displayed enethiolization in solution,[48] leading to an equilibrium between the thione and thiol forms (Scheme 2 and Scheme S4, see SI), a common phenomenon observed in similar compounds. This tautomeric behaviour may influence the ligand's coordination properties, contributing to the stability and reactivity of the resulting organotin(IV) complexes. The potassium salt of the ligand was synthesised by treating the ligands with KOH (1.0 equivalent) in methanol. Deprotonation leads to stabilization of the thiol tautomer, and in contrast to the neutral ligand, the salt exists exclusively in the thiol form.



Scheme 2 Thione-thiol tautomerism observed in compound **H_2L**.

This journal is © The Royal Society of Chemistry 2026

We have selected organometallic Bu_2SnCl_2 or Ph_2SnCl_2 as the metal precursor due to their known anticancer activity; however, these compounds exhibit cytotoxicity toward both normal and cancer cells. The coordination environment of the metal center play a vital role in the anticancer activity, and metal center of the active organotin compounds have several key features such as open coordination sites at Sn, relatively stable bonds between the ligand and Sn, particularly Sn–N and Sn–S, and slow hydrolysis of these bonds in aqueous environments.[27] Therefore, we reacted these precursors with our multifunctional ligand (**L**) to get a different coordination environment and geometry. The differences in the coordination geometries around the metal center and the formation of Sn–N and Sn–S bonds could alter their biological properties, which may enhance the anticancer activities and reduce their cytotoxicity towards normal cells. Coordination of this ligand to the metal centers of Bu_2SnCl_2 or Ph_2SnCl_2 proceeded through chloride ion release, resulting in the formation of Bu_2SnL and Ph_2SnL complexes (Scheme 3 and Scheme S3, see SI). The synthesised compounds were characterised by standard analytical techniques (Fig. S1–S38, see SI) such as ^1H, ^{13}C, and ^{31}P NMR spectroscopy, CHN analysis, infrared (IR) spectroscopy, and electrospray ionization mass spectrometry (ESI-MS). The NMR spectra confirmed the presence of both the thione and thiol tautomers of **PL**, with the thione form predominant.

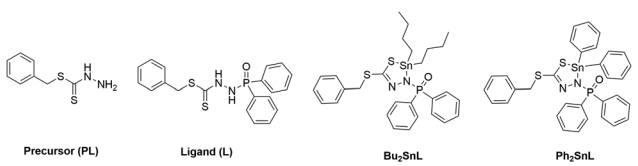
The ^1H NMR spectrum of **PL** showed two resonances corresponding to the benzyl protons at 4.36 ppm (thiol) and 4.39 ppm (thione) (Fig. S1, see SI). Similarly, the ^1H NMR spectrum of $\mathbf{H_2L}$ exhibited duplicated signals for several protons (Fig. S5, see SI), with the benzyl methylene protons clearly resolved at 4.43 ppm for the thione form and 4.46 ppm for the thiol form. The ^{13}C NMR spectrum showed two signals for the benzyl carbon at 37.57 and 37.81 ppm (Fig. S7, see SI), consistent with the ^1H NMR spectrum. The resonance at 21.39 ppm in ^{31}P NMR corresponds to the thione tautomer, and the signal at 20.93 ppm is assigned to the thiol form (Fig. S9, see SI). The NMR spectra of the metal complexes displayed single resonances, indicating the absence of tautomerism due to coordination-induced structural rigidity (Fig. S15–S26, see SI). The ^{119}Sn NMR spectra of the Bu_2SnL and Ph_2SnL show resonances at δ −4.36 ppm and δ −144.47 ppm, respectively, consistent with four-coordinate tetrahedral geometries in both cases (Fig. S20 and S26, see SI).[49] The significant upfield shift observed for the diphenyltin derivative reflects the stronger electronic influence of phenyl groups compared to the butyl substituents.[50] ^{119}Sn NMR spectra of the precursors Bu_2SnCl_2 and Ph_2SnCl_2 were consistent with literature reports,[51] indicating DMSO-coordinated species, which was evident from the broad peaks and the observed upfield shifts (Fig. S27 and S28, see SI).

Infrared (IR) spectroscopy was employed to identify major absorption peaks in the compounds, confirming their proposed structures (Fig. S34–S38, see SI). A distinct peak at 1043.81 cm^{-1} in **PL** indicates the presence of the C═S group. Upon formation of the $\mathbf{H_2L}$, a new peak appears at 1189.10 cm^{-1}, indicative of the P═O bond. The C═S peak remains relatively unchanged at 1050.99 cm^{-1}. The absence of ν(S–H) in the IR spectrum shows that $\mathbf{H_2L}$ exists only in the thione form in the solid state. The disappearance of the C═S and N–H peaks in tin(IV) complexes suggests successful coordination of $\mathbf{H_2L}$ to the metal center. The shift in the P═O peak towards lower wavenumbers may be attributed to the polymeric structure, as confirmed by X-ray crystallography. These observations further substantiate the formation and structure of the tin-ligand complexes.

X-ray diffraction

The crystallographic data and the hydrogen bonding parameters are provided in Tables S1 and S2 (see SI). X-ray quality crystals of the **PL** and $\mathbf{H_2L}$ were obtained by keeping concentrated hot dichloromethane and methanolic solutions in a refrigerator overnight, respectively. Single crystal X-ray diffraction analysis revealed that compounds **PL** and $\mathbf{H_2L}$ crystallized in a $P2_1/c$ space group, and the structural analysis revealed the thione form in the solid-state structures (Fig. 1A and Fig. S39, see SI). In the crystal structure, compound $\mathbf{H_2L}$ displayed a hydrogen-bonded dimer, whereas compound **PL** showed a 1-D hydrogen-bonded chain (Fig. S39, see SI). The crystals of Bu_2SnL and Ph_2SnL were obtained by cooling a hot methanolic solution of the complexes in the refrigerator overnight.

Single-crystal X-ray diffraction revealed that Bu_2SnL crystallized in the monoclinic $C2/c$ space group and Ph_2SnL in an orthorhombic *Pbca* space group. The structural analysis of the complexes indicated that the tin(IV) metal centers were coordinated to ligand **L** in a chelate fashion *via* the nitrogen and sulfur atoms, as well as the carbon atoms of the butyl/phenyl groups. The tin(IV) metal center adopted a distorted trigonal bipyramidal geometry in both structures (Fig. 1B & C), and the coordination of the phosphine oxide of the adjacent ligand to the metal center resulted in 1-D coordination polymers (Fig. S40 & S41, see SI). The interaction between the tin(IV)



Scheme 3 Chemical structure of the precursor, ligand and tin(IV) complexes.

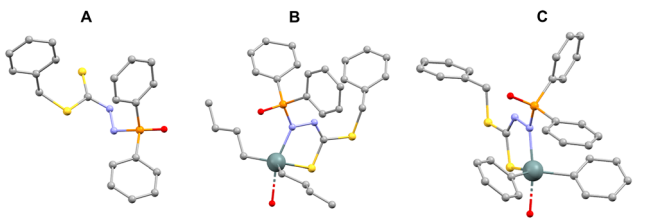


Fig. 1 Crystal structure of (A) compound $\mathbf{H_2L}$, (B) Bu_2SnL, and (C) Ph_2SnL, colour code: carbon (light grey), nitrogen (dark blue), oxygen (red), phosphorus (orange), and tin (teal).

metal center and the oxygen atom of phosphine oxide demonstrates the accessibility of the metal center, which might enhance its reactivity and ability to binding to the biological targets. The ligand adopted a thiol form in both structures, presumably due to metal coordination, which is evident from the bond lengths (Table S3, see SI). In Bu_2SnL, one of the phenyl groups of the phosphine oxide moiety and the phenyl moiety of **L** were disordered. The solvent water molecule in Ph_2SnL was found to be severely disordered and the solvent contribution was excluded using PLATON/SQUEEZE.[52] The selected bond lengths and angles of the metal centers in the tin(IV) complexes are provided in Table S4 (see SI). The phase purity of all crystals was analysed by comparing powder X-ray diffraction (PXRD) patterns[53] of the bulk materials with simulated patterns derived from the respective crystal structure (Fig. S42–S45, see SI).

Stability studies

Metal complexes can interact with solvents/media, leading to ligand exchange reactions even before the experiments begin.[54] The presence of water in cell culture media or cellular fluids can similarly coordinate (*via* oxygen atom) with tin(IV) complexes and degrade the metal complexes. Thus, it is crucial to evaluate the stability of the tin(IV) complexes in the stock solution and aqueous environment. The NMR experiments in DMSO-d_6 provide information about the intrinsic chemical stability of the complex in the stock solution, and NMR in aqueous DMSO-d_6 could check the possibility of water-mediated degradation pathways possible in cellular media. The stability of tin(IV) complexes was analysed in both DMSO and aqueous DMSO (9 : 1, v/v, DMSO-d_6/D_2O) solutions using NMR spectroscopy, and the results indicated that the tin (IV) complexes were stable in both DMSO-d_6 and DMSO-d_6/D_2O (9 : 1, v/v) for at least seven days, as no spectral changes were observed during this period (Fig. S46–S61, see SI). The sharp and relative downfield ^{119}Sn NMR signals indicate that there is no DMSO coordination, unlike the corresponding tin precursors (Bu_2SnCl_2 and Ph_2SnCl_2). This highlights the stabilizing role of the ligand in our complexes, which maintains the four-coordinate tetrahedral geometry around the tin center. The stability of the tin complexes suggests that these compounds could enter the cells without undergoing structural alterations, making them promising candidates for biological studies.

Evaluation of anticancer activity

To further evaluate the potential of our tin(IV) complexes as chemotherapeutic agents, we conducted cytotoxicity assays *in vitro*. The purity of the complexes was confirmed by elemental analysis, and only crystalline pure complexes were used in biological assays. The half-maximal inhibitory concentration (IC_{50}) of the tin(IV) complexes was assessed against a range of cancer (HCT116, AsPC-1, T-47D) and non-cancer (HEK293T) cell lines using the standard MTT cytotoxicity assay, a colorimetric method to determine mitochondrial activity. The MTT assay is widely used to evaluate the *in vitro* cytotoxic effects of drugs on cell lines because the total mitochondrial activity generally correlates with the number of cells.[55]

The tin(IV) complexes demonstrated significant cytotoxicity across all tested cancer cell lines (Table 1), and the dibutyltin complex (Bu_2SnL) exhibits notably higher potency than the diphenyltin complex (Ph_2SnL), the ligand, and cisplatin. This effect was particularly evident in the human breast cancer T-47D cell line, where cisplatin showed limited efficacy (28.23 ± 0.49 μM), Ph_2SnL showed moderate cytotoxicity (1.25 ± 0.04 μM), and Bu_2SnL displayed the highest toxicity (0.32 ± 0.04 μM). This observation suggests a unique mechanism of action for Bu_2SnL, making it a promising alternative to platinum-based drugs or a candidate for combination therapy. The improved performance of the Bu_2SnL complex is attributed to the electronic and steric properties of the butyl substituents, which can enhance lipophilicity and facilitate cellular uptake, as well as influence the coordination environment and reactivity of the tin center. In contrast, the bulkier and more rigid phenyl groups may limit accessibility to biological targets and alter interaction profiles and similar trends have been reported in the literature (Table S5, see SI). As anticipated, the ligand alone exhibited only mild toxicity (IC_{50} > 100 μM), underscoring the critical roles of the tin metal center and the ligand in the organometallic complexes in mediating the cytotoxicity of the complex. To justify the structural design for therapeutic applications, we analysed the toxicity of the complexes towards non-cancerous cells and the tin(IV) complexes displayed lower toxicity towards non-tumorigenic epithelial cell line HEK293T (IC_{50} = 0.59 ± 0.07) compared to T-47 cancer cell line, indicating that they might be slightly selective for malignant cells (refer to Fig. S62–S65 for dose-dependent viability data, see SI). Although HEK293T cells provide preliminary evidence of mild selectivity, these transformed cells do not accurately represent normal human tissue. In order to get a better understanding of the therapeutic potential of the tested compounds, further studies with non-transformed normal human cell lines and *in vivo* models are required. We also performed the cytotoxicity assays for tin precursors (Bu_2SnCl_2 and Ph_2SnCl_2) (Table S6 and Fig. S66–S69, see SI). Although their cytotoxicity values were not dramatically different from those of our complexes, the precursors were more toxic toward non-cancerous

Table 1 IC_{50} (μM) of compounds against various cell lines

IC_{50}	HCT116+ Chr.3	AsPC-1	T-47D	HEK293T
Bu_2SnL	1.56 ± 0.07	1.55 ± 0.11	0.32 ± 0.04	0.59 ± 0.07
Ph_2SnL	4.32 ± 0.30	4.16 ± 0.26	1.25 ± 0.04	2.47 ± 0.17
Cisplatin	12.89 ± 0.61	6.07 ± 1.17	28.23 ± 0.49	8.25 ± 0.47
Ligand	146.63 ± 15.01	146.89 ± 10.60	116.95 ± 5.56	100.91 ± 3.77

This journal is © The Royal Society of Chemistry 2026

HEK293T cells. For example, Bu_2SnL shows an IC_{50} of 0.59 ± 0.07 in non-cancerous HEK293T compared to 0.38 ± 0.04 for Bu_2SnCl_2. These results indicate the incorporating multifunctional groups could reduce the toxicity towards non-cancerous cell line, which underscores the protective and modulatory role of the ligand in our complexes, complementing the DMSO stability observed earlier.

Lipophilicity studies

Lipophilicity is a critical factor in pharmacology, affecting essential properties of a drug, such as membrane permeability, biodistribution, and metabolism.[56] The lipophilic interactions of the complexes are highly dependent on the ligand moiety and the alkyl/aryl substituents attached to the tin metal center. To assess the lipophilicity profile of the synthesised tin(IV) complexes, we utilized the shake-flask method based on *n*-octanol/water partitioning. ICP-MS partitioning results revealed that the Bu_2SnL complex possesses greater lipophilicity ($\log P_{o/w}$ = 2.26 ± 0.05) compared to the Ph_2SnL complex ($\log P_{o/w}$ = 2.07 ± 0.04); nevertheless, both complexes fall within the optimal lipophilicity range for orally administered drugs, indicating their suitability for further biological assays (Fig. 2A and Table S7, see SI). Literature reports indicate a linear relationship between lipophilicity and cytotoxicity, wherein dibutyltin complexes are more cytotoxic than diphenyl tin-based systems.[57] We observed the same observations and found dibutyl tin is more lipophilic than diphenyl tin complexes, which makes them more cytotoxic.

Whole cell uptake and cellular localization

Efficient cellular delivery is essential in drug development, as the plasma membrane serves as the primary barrier that drugs must cross to achieve optimal bioavailability. In general, lipophilicity and whole-cell uptake are closely correlated, as lipophilic small molecules can more readily cross lipid bilayers through passive diffusion facilitated by hydrophobic interactions, which is highly dependent on ligand attached to metal centre. Based on their superior cytotoxicity and selectivity, T-47D cells were selected for subsequent whole-cell uptake and biological studies. After incubating at 1.0 μM in T-47D cells for 24 h, the whole-cell uptake of complex Bu_2SnL (13.3 ± 2.2 fg per cell) was found to be significantly greater than that of Ph_2SnL (7.7 ± 1.5 fg per cell). We found that Bu_2SnL has higher whole-cell uptake than Ph_2SnL; this result aligns with the well-established correlation between increased lipophilicity and enhanced cellular uptake[57] (Fig. 2B and Table S8, see SI).

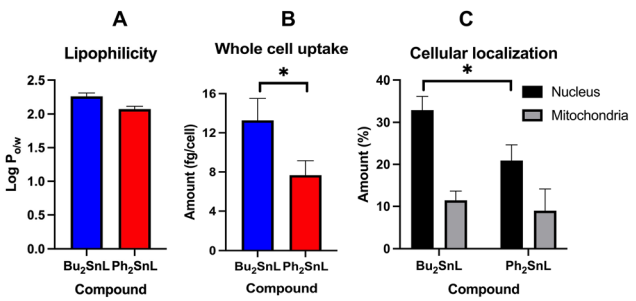


Fig. 2 (A) Lipophilicity of the tin complexes; (B) whole cell uptake of tin (IV) complexes; (C) cellular localization of tin(IV) in T-47D cells inside the major cellular organelles (nucleus and mitochondria) after 24 h incubation (n = 3, *p < 0.05).

To investigate the fate of organotin complexes after traversing cellular membranes and to identify their subcellular targets and molecular mechanisms of action, we performed subcellular localization assays. Cellular localization was assessed by extracting the nucleus and mitochondria after treatment with organotin complexes, and the tin content within the organelles was quantified using inductively coupled plasma mass spectrometry (ICP-MS). Both complexes were found to localize in the nucleus, with Bu_2SnL exhibiting an accumulation of 32.9 ± 3.3%, while Ph_2SnL showed a lower accumulation of 20.9 ± 3.7% (Fig. 2C). Substantial levels of the tin-metal were detected in the nucleus of cells treated with Bu_2SnL, suggesting that specific interactions drive nuclear localization. This nuclear accumulation implies that nucleic acids, especially DNA, may serve as one of the primary intracellular targets, potentially contributing to the observed cytotoxic effects. The lack of mitochondrial accumulation suggests that mitochondria are unlikely to be the primary cellular target of the tin complexes. Collectively, these findings indicate that both the lipophilic nature of the complex and its nuclear targeting ability play crucial roles in mediating its biological activity.

Cell cycle modulation

The cell cycle consists of a tightly regulated sequence of cellular events, including checkpoints that control progression between different phases, particularly under stress conditions. Choroba *et al.* report that upon accumulation of their complexes in the nucleus, interphase check points induce cell cycle arrest, facilitate DNA repair, and trigger apoptosis.[58] The nuclear localization of the tin(IV) complex suggests a potential interaction with DNA that might trigger the cell cycle arrest. To investigate this possibility, cell cycle analysis was performed using flow cytometry (Fig. 3 & Fig. S70, Table S9, see SI). The cytotoxic effects of tin(IV) complexes, the ligand, and cisplatin, and their influence on cell cycle progression were evaluated using propidium iodide (PI). This DNA-intercalating fluorophore enables quantification of cellular DNA content across the different phases of the cell cycle (G0/G1, S, and G2/M), as PI fluorescence intensity increases proportionally with DNA duplication from G1 to G2 phase.

As illustrated in Fig. 3, treatment with Bu_2SnL resulted in cell cycle arrest (12.0% increase) at the G0/G1 phase when administered at a concentration of 0.3 μM for 24 h in the T-47D cell line. By inducing this G0/G1 cell cycle arrest by Bu_2SnL, DNA synthesis might be impaired, thereby suppressing uncontrolled tumour cell proliferation, a fundamental hallmark of malignant tumours. In contrast, the other compounds tested at the same concentration exhibited negligible

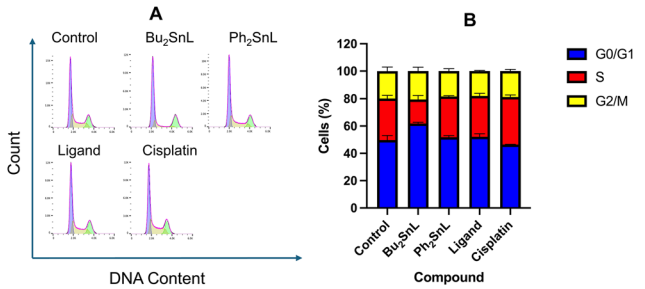


Fig. 3 (A) Cell cycle arrest of T-47D cells and cell cycle distribution after incubation with compounds (0.3 μM) for 24 h; (B) change in G0/G1, G2/M, and S phase.

effects on cell cycle progression. Notably, while cisplatin is known to induce cell cycle arrest in the S phase, our compound appears to arrest specifically in the G0/G1 phase. This observation suggests the possibility of distinct mechanisms of action, despite both agents targeting the nucleus.

Effect of organotin(IV) complexes on cell death processes

The cellular response to cell cycle arrest can often lead to the induction of apoptosis. Apoptosis is a tightly regulated form of programmed cell death triggered by cellular stress or damage, characterised by phosphatidylserine externalization, membrane blebbing, chromatin condensation, and DNA fragmentation.[59] To investigate this potential outcome, we performed an Annexin V-FITC/PI flow cytometry assay, which allows differentiation between apoptotic and necrotic cells based on characteristic membrane changes. Our analysis revealed that the dibutyl tin(IV) complex effectively induces apoptosis in T-47D cancer cells after treatment at 5.0 μM for 4 h. Specifically, we observed an increase in the population of Annexin V-positive cells (37.5 ± 9.6%) compared with the control (5.1 ± 0.1%), indicating activation of the apoptotic pathway (Fig. 4). These findings suggest that the Bu_2SnL complex triggers programmed cell death, contributing to its cytotoxic effects against cancer cells.

Cellular ROS generation

The Reactive oxygen species (ROS), including superoxide anions, hydrogen peroxide, and hydroxyl radicals, play a dual role in cancer biology. At moderate levels, ROS function as signalling molecules that promote cell proliferation and survival; however, excessive ROS accumulation induces oxidative stress, leading to DNA damage, mitochondrial dysfunction, and activation of apoptotic pathways.[60] Intracellular ROS levels were assessed using the 2′,7′-dichlorofluorescein diacetate (DCFH-DA) assay. Upon oxidation by reactive oxygen species, DCFH is converted to the highly fluorescent 2′,7′-dichlorofluorescein (DCF), which can be quantified by fluorescence spectroscopy or flow cytometry.[61]

No detectable ROS production was observed in T-47D cells after 4 h of treatment with the complexes (Fig. S71, see SI). This absence of ROS generation aligns with our whole-cell

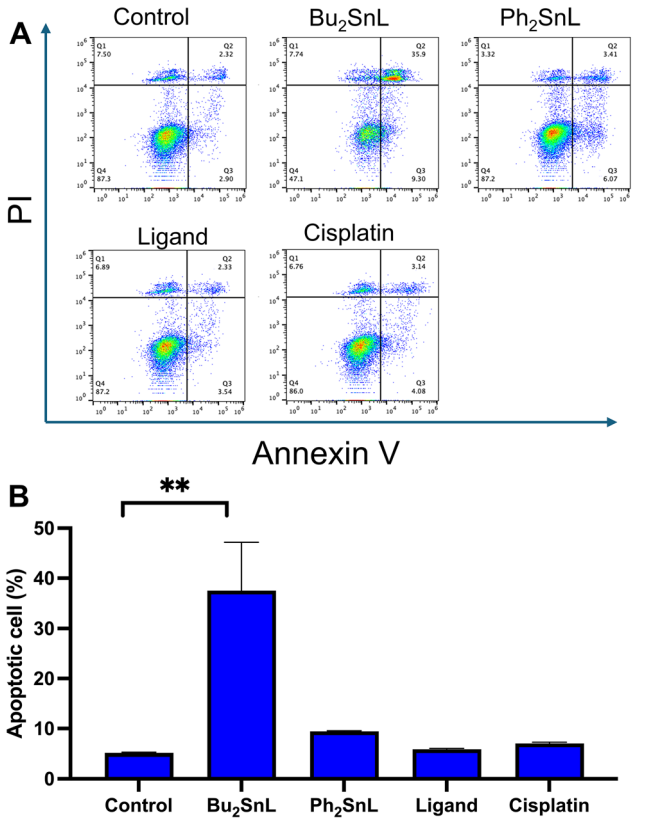


Fig. 4 (A) Flow cytometry of Annexin V/PI-stained T-47D cells incubation with compounds (5.0 μM) for 4 h; (B) bar graph illustrating the apoptotic cell population after incubation with compounds (5.0 μM) for 4 h (n = 3, $^{**}p < 0.01$).

uptake studies, which showed that the complexes do not specifically localize in mitochondria, the primary site of intracellular ROS production. Their limited mitochondrial accumulation likely prevents meaningful interactions with the electron transport chain, thereby having little effect on the production of superoxides or downstream peroxides.

Cellular ATP depletion

Adenosine triphosphate (ATP) serves as the central energy currency of the cell, driving numerous biochemical and metabolic processes.[62] Complexes that disrupt cellular metabolism often cause a reduction in ATP levels, thereby compromising energy-dependent functions and promoting apoptosis or other forms of cell death. Intracellular ATP levels are closely associated with cellular viability and were quantified using a luminescence-based ATP detection assay. To evaluate the contribution of ATP depletion to the mechanism of action of the complexes, cells were treated at their respective IC_{50} and $2 \times IC_{50}$ concentrations. All compounds (Bu_2SnL, Ph_2SnL and cisplatin) induced reduction in intracellular ATP levels; however, the extent of ATP depletion was moderate and markedly less pronounced than that typically observed for metabolic or mitochondrial-targeting agents (Fig. S72 and Table S10, see SI). The observed decrease in ATP content correlated with reduced

This journal is © The Royal Society of Chemistry 2026

cell viability, indicating an association between energy status and cytotoxicity. However, the absence of severe ATP depletion suggests that disruption of cellular energy metabolism is unlikely to be the primary cause of the cell death induced by these complexes.

Mechanism of action

The nuclear accumulation of tin(IV) complexes, revealed by subcellular localization analysis, demonstrates their potential to interact with DNA. This prompted us to perform various Drug-DNA interactions studies. Competitive fluorescence displacement assays using 4′,6-diamidino-2-phenylindole (DAPI) and ethidium bromide (EB) were employed to differentiate DNA binding modes of the complexes. The DAPI preferentially binds in the minor groove of duplex DNA, resulting in enhanced fluorescence that is reduced upon displacement by groove-binding compounds. On the other hand, EB intercalates between base pairs and its fluorescence decreases upon displacement by intercalative compounds, thereby enabling discrimination between groove binding and intercalation interactions.[63,64] We have performed DAPI or EB displacement assays to check whether there is DNA groove binding or intercalation. No significant spectral changes were observed in DAPI or EB displacement assays with Bu_2SnL. The unchanged fluorescence profiles indicate that the complexes do not displace these canonical DNA-binding dyes, implying Bu_2SnL is not interacting with DNA either *via* intercalation or groove binding (Fig. S73 & S74, see SI). This observation is consistent with previous reports, supporting the fact that the tin(IV) complexes might bind selectively to the phosphate groups of the DNA backbone.[37]

The oxygen atoms of the phosphate groups are classified as hard Lewis bases; consequently, they preferentially interact with hard Lewis acids such as metal at higher oxidation state (Sn^{4+}).[65] Organotin(IV) compounds are well known for their hypervalent coordination behaviour, which enables them to accommodate additional donor ligands, including phosphates, and to adopt higher coordination numbers (CN > 4).[66,67] To confirm this interaction, we reacted equimolar amounts of Bu_2SnL and potassium ethyl phosphonate (EtOPH(O)OK), and the subsequent ESI-MS analysis revealed the formation of coordination complex including both the species (Fig. S75, see SI). We performed NMR experiments to validate this observation by adding phosphonate (0.1–5.0 equivalent) to a DMSO-d_6 solution of Bu_2SnL. ^{119}Sn NMR spectra exhibited pronounced upfield shifts (−4.22 to −82.32 ppm) upon phosphonate addition, indicating a transition of the tin(IV) complex from four- to five-coordinate geometry[68] and the complex formation (Fig. 5 and S76, see SI).

The addition of phosphonate (0.1 equivalent) resulted in broadening the peak for the four-coordinate species in the ^{119}Sn NMR spectrum, which disappeared upon increasing the phosphonate concentration (0.5 equivalent). The phosphonate concentration (1.0 equivalent) was further increased, leading to the formation of a broad signal that corresponds to five-coordinated species (Fig. S76, see SI). This indicates a dynamic

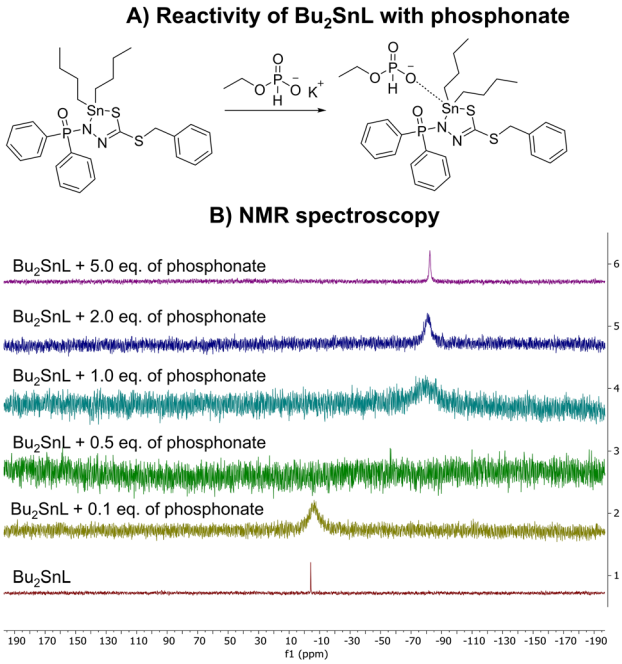


Fig. 5 Representation of the Bu_2SnL-phosphonate adduct, (A) proposed reaction scheme of Bu_2SnL and phosphonate; (B) ^{119}Sn NMR of the mixture of Bu_2SnL and phosphonate in DMSO-d_6.

equilibrium between free and bound species, as evidenced by the gradual shifts in the phosphorus signals in ^{31}P NMR spectra (Fig. S77, see SI). The disappearance of the peaks at 0.5 equivalent of phosphonate prompted us to check whether the equilibrium is time-dependent using ^{119}Sn and ^{31}P NMR experiments, which revealed that the equilibrium is established rapidly (Fig. S78 and S79, see SI). To mimic interactions of the metal complexes with the DNA nucleotide moiety, NMR experiments were performed with guanosine monophosphate (GMP) triethylammonium salt and Bu_2SnL, which displayed clear changes in both the ^{31}P and ^{119}Sn NMR spectra (Fig. S80 and 81, see SI). These results were similar to the NMR experiments with phosphonate, confirming that the metal center interacts with the phosphate group. The ^{119}Sn NMR signal broadened and eventually disappeared, suggesting that the metal center interacts with the GMP. The absence of the signal corresponding to a five-coordinated tin species even at higher equivalence of GMP may be attributed to the ligand exchange process, which was confirmed by the presence of anionic free ligand (18–19 ppm) in the ^{31}P NMR spectrum. NMR experiments performed by adding diethyl phosphite devoid of an anionic oxygen atom to the Bu_2SnL solution (Fig. S82 and S83, see SI) indicated no changes in the spectra. This shows the importance of the anionic oxygen atom in phosphate moieties and confirms that the phosphate anionic oxygen atom is coordinated to the tin metal center. The possibility of the metal center interacting with the nucleobase and sugar moieties of DNA was ruled out by performing a similar NMR experiment with 2′-deoxyguanosine, which showed no significant chemical shift changes or signal broadening (Fig. S84 and S85, see SI).

These results indicate that Bu_2SnL might have more affinity for the DNA phosphate backbone over other conventional binding modes. A similar five-coordinate phosphonate-bound species was also observed for Ph_2SnL, but the absence of a sharp and intense ^{119}Sn NMR peak suggests that the phosphate-binding ability of Ph_2SnL was relatively weak compared to Bu_2SnL, which can be correlated to their relative anticancer activity (Fig. S86 and 87, see SI). Additionally, no five-coordinate species was formed upon addition of 1.0 equivalent of phosphonate to the tin precursors (Bu_2SnCl_2, and Ph_2SnCl_2), highlighting the critical role of the ligand in the metal complex for phosphate binding (Fig. S88 and 89, see SI).

The organometallic complex-DNA interactions often lead to cellular DNA damage, and we performed the comet assay, or single-cell gel electrophoresis, a sensitive and widely used technique for detecting DNA damage at the individual-cell level.[69] By embedding cells in agarose, lysing them, and applying electrophoresis, fragmented DNA migrates to form a characteristic "comet" tail, the length and intensity of which quantitatively reflect the extent of DNA strand breaks. As shown in Fig. 6A, fluorescent microscopy revealed comet formation in cells treated with Bu_2SnL. The extent of DNA migration increased in a time-dependent manner, with quantification (Fig. 6B and C) showing significant elevations in both tail DNA and Olive moment.

These findings indicate that Bu_2SnL induces moderate to severe DNA damage, suggesting that its cytotoxic effects may be mediated, at least in part, through interacting with DNA. The observed DNA damage caused by Bu_2SnL to T-47D cells identifies the possibility of DNA as one of the key targets. These findings support the hypothesis that tin(IV) complexes accumulate in the nucleus, which might bind to the DNA phosphate backbone, likely inducing conformational changes or DNA condensation that could disrupt DNA integrity, causing damage and loss of function. Such disruption may ultimately lead to intracellular ATP depletion, cell cycle arrest and cell death, highlighting the potential of these complexes as agents for targeting nuclear DNA and advancing anticancer research.

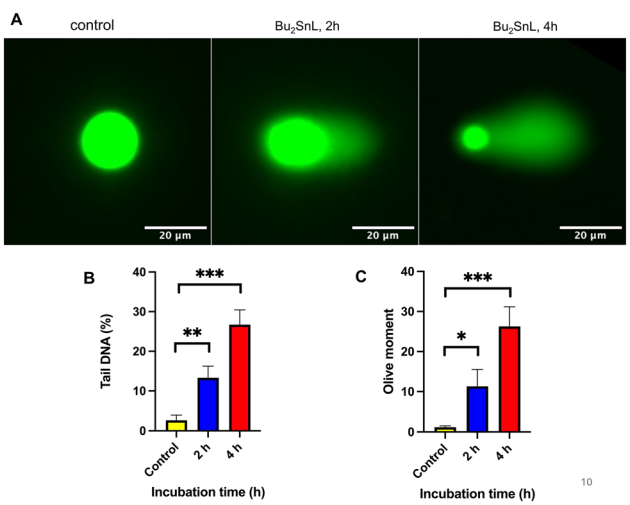


Fig. 6 T-47D cells incubated with Bu_2SnL for 2.0 and 4.0 h: (A) comet assay performed by fluorescence microscopy with comet dye staining; (B) tail DNA (%) of the cell. (C) olive moments of the cell (n = 3, *p < 0.05, **p < 0.01, ***p < 0.001).

Conclusions

In this study, we report the synthesis and biological evaluation of two organotin(IV) complexes (Bu_2SnL and Ph_2SnL) with multifunctional groups. Our strategy was to synergistically combine the intrinsic cytotoxic potential of the organotin(IV) center with multifunctional ligands containing functional moieties that could enhance the anticancer efficacy, which may induce distinct DNA-binding modes. Bu_2SnL exhibited a broad-spectrum antiproliferative activity across multiple cancer cell lines, significantly surpassing cisplatin under comparable conditions. The cellular and mechanistic studies indicate that Bu_2SnL preferentially accumulates in the nucleus and are proposed to interact with DNA *via* coordination to external phosphate groups, as characterised by NMR spectroscopy and mass spectrometry, rather than through classical intercalation. The proposed interaction is consistent with the observed induction of DNA damage and arrest at the G1 phase, ultimately leading to apoptosis-mediated cell death. We have shown that the combination of a multifunctional ligand with the Lewis acidic and hyper coordination properties of organotin(IV) could facilitate the proposed DNA phosphate-binding mode. The proposed mode of action could distinguish these organotin(IV) complexes from existing DNA-targeting metal-based chemotherapeutics, thereby enhancing their anticancer efficacy, supporting the advancement of alternative DNA-binding cancer agents. In summary, these findings suggest Bu_2SnL as a promising lead compound and highlight organotin(IV) frameworks as a valuable and underexplored chemical space for anticancer drug discovery. Ongoing studies focus on elucidating the precise molecular basis of cellular DNA recognition, defining the contributions of individual structural moieties to biological activity, and optimizing the pharmacological profile to support future preclinical development.

Experimental

Materials and methods

All starting materials and solvents were purchased from commercial sources and used as supplied. The tin(IV) complexes Bu_2SnCl_2 and Ph_2SnCl_2 were purchased from TCI Chemical Trading Co., Ltd. NMR and IR spectra were recorded on a Bruker AVANCE 400 spectrometer and a Nicolet iS10 FT-IR spectrometer, respectively. Electrospray ionization mass spectra (ESI-MS) were recorded on the Bruker Compact QTOF mass spectrometer. Elemental analyses were carried out on an Elementar Analysensysteme GmbH Vario EL V3.00 and Vario EL Cube. Bruker D8 venture and PANalytical X-ray diffraction

This journal is © The Royal Society of Chemistry 2026

(XRD) instruments were used for the single-crystal (SCXRD) and powder (PXRD) diffraction experiments, respectively. Inductively coupled plasma mass spectrometry (ICP-MS) measurements have been recorded on an iCAP RQ (Thermo Fisher) spectrometer. The absorption within 96 well plates was measured using an EMax Plus microplate reader. Flow Cytometry was performed on a Attune™ NxT Acoustic Focusing Cytometer or BD FACSymphony flow cytometer (BD Bioscience). For all biological experiments, DMSO concentration was 0.05% or less, unless otherwise specified.

Synthesis

Synthesis of potassium hydrazinecarbodithioate. The synthesis was carried out following a modified procedure reported in the literature.[47] Hydrazine monohydrate (1.45 mL, 30.0 mmol) was dissolved in 20.0 mL of 1,4-dioxane in a 100 mL round-bottom flask. Potassium hydroxide (1.68 g, 30.0 mmol) was added to the solution, and the mixture was stirred at room temperature for 10 minutes under a nitrogen atmosphere. After the initial mixing period, a solution of carbon disulfide (1.81 mL, 30.0 mmol) in 20.0 mL of 1,4-dioxane was added dropwise to the reaction mixture while maintaining the temperature at 0 °C using an ice bath. The reaction mixture was stirred for an additional 2 h at 0 °C, resulting in the formation of a white precipitate. The precipitate was collected by filtration, washed with 1,4-dioxane and diethyl ether, and then dried under vacuum to afford the crude product. The product was used in the next step without further purification.

Synthesis of benzyl hydrazinecarbodithioate (PL). To a solution of potassium hydrazinecarbodithioate (30.0 mmol, 1.5 equivalent) in a 1 : 2 water–methanol mixture (30.0 mL), a solution of benzyl bromide (2.37 mL, 20.0 mmol, 1.0 equivalent) in methanol (20.0 mL) was added dropwise over 20 minutes. The reaction mixture was stirred at room temperature for 16 h. After completion, methanol was evaporated under reduced pressure. The resulting aqueous mixture was sequentially washed with 0.5 N HCl (40.0 mL) and saturated $NaHCO_3$ solution (40.0 mL). The organic product was then extracted with dichloromethane (3 × 40.0 mL). The combined organic layers were washed with saturated brine solution, dried over anhydrous $MgSO_4$, filtered, and concentrated under vacuum to yield a white powder. The crude product was further purified by column chromatography using silica gel as stationary phase and methanol/dichloromethane mixture as the eluent, affording the desired product as a white powder in 80.18% yield (3.18 g, 16.03 mmol). Colourless crystals suitable for X-ray crystallography were obtained by keeping a concentrated hot solution of the product in dichloromethane in a refrigerator overnight. ^{1}H NMR (400 MHz, DMSO-d_6) δ 10.86 (s, 1H), δ 7.38–7.34 (m, 2H), 7.32–7.27 (m, 2H), 7.23 (tdd, J = 7.4, 4.0, 2.5 Hz, 1H), 5.11 (s, 2H), 4.39 (s, 2H). ^{13}C NMR (101 MHz, DMSO-d_6) δ 199.85, 137.79, 128.87, 128.34, 126.92, 37.06. MS-ESI(m/z) calc. for $C_8H_{10}N_2NaS_2^+$ $[M + Na]^+$: 221.0178, found 221.0169. Elemental analysis: C, 48.46; H, 5.08; N, 14.13. Found: C, 48.44; H, 4.70; N, 14.07.

Synthesis of benzyl 2-(diphenylphosphoryl)hydrazine-1-carbodithioate (H_2L). Compound **PL** (0.99 g, 5.0 mmol) was added to a 100 mL oven-dried two-neck round-bottom flask, which was then evacuated and flushed with nitrogen three times. Dry dichloromethane (20.0 mL) was added to the flask, followed by the slow addition of triethylamine (0.84 mL, 6.0 mmol, 1.2 equivalent). The reaction mixture was stirred for 10 minutes in an ice bath. Subsequently, a solution of diphenyl phosphinic chloride (1.05 mL, 5.5 mmol, 1.1 equivalent) in dichloromethane (20.0 mL) was added dropwise over 30 minutes. The reaction was allowed to proceed at room temperature with continuous stirring for 16 h. Upon completion, the reaction mixture was washed sequentially with 0.5 N HCl (30.0 mL) and saturated $NaHCO_3$ solution (30.0 mL). The organic phase was extracted with dichloromethane (2 × 30 mL), washed with saturated brine solution, dried over anhydrous $MgSO_4$, filtered, and concentrated under vacuum to yield a white powder. The crude product was purified by column chromatography using a 1 : 1 mixture of ethyl acetate and petroleum ether as the eluent, yielding the desired product as a white powder (yield: 70.26%, 1.4 g, 3.5 mmol). A concentrated hot methanolic solution of the product was placed in a refrigerator overnight, yielding colourless X-ray-quality single crystals. ^{1}H NMR (400 MHz, DMSO-d_6) δ 11.47 (s, 1H), 8.64 (d, J = 16.5 Hz, 1H), 7.85 (ddt, J = 11.9, 6.9, 1.4 Hz, 4H), 7.58 (dddd, J = 9.1, 5.3, 3.4, 1.9 Hz, 2H), 7.49 (ddd, J = 8.8, 6.7, 3.4 Hz, 4H), 7.32–7.24 (m, 5H), 4.43 (s, 2H). ^{13}C NMR (101 MHz, DMSO-d_6) δ 203.47 (d, J = 4.0 Hz), 137.27, 132.24 (d, J = 2.9 Hz), 131.93 (d, J = 9.7 Hz), 130.88 (d, J = 126.2 Hz), 128.95, 128.47 (d, J = 12.5 Hz), 128.36, 127.03, 37.57. ^{31}P NMR (162 MHz, DMSO-d_6) δ 21.39. MS-ESI(m/z) calc. for $C_{20}H_{19}N_2NaOPS_2^+$ $[M + Na]^+$: 421.0569, found 421.0565. Elemental analysis: C, 60.28; H, 4.81; N, 7.03. Found: C, 60.27; H, 4.78; N, 7.00.

Synthesis of K+ salt of the ligand. A solution of KOH (28.0 mg, 0.5 mmol, 1.0 equivalent) in methanol (1.0 mL) was added dropwise to a solution of the compound **H_2L** (199.2 mg, 0.5 mmol) in methanol (10.0 mL). The resulting mixture was stirred at room temperature for 10 minutes and was dried to obtained product in equimolar yield. ^{1}H NMR (400 MHz, DMSO-d_6) δ 8.58 (d, J = 20.0 Hz, 1H), 7.81–7.75 (m, 4H), 7.56–7.45 (m, 6H), 7.13–7.05 (m, 5H), 3.94 (s, 2H). ^{13}C NMR (101 MHz, DMSO-d_6) δ 162.21, 140.55, 133.79 (d, J = 126.8 Hz), 131.75 (d, J = 9.1 Hz), 131.28 (d, J = 2.9 Hz), 128.83, 128.28 (d, J = 12.0 Hz), 127.82, 125.84, 34.26. ^{31}P NMR (162 MHz, DMSO-d_6) δ 18.30. MS-ESI(m/z) calc. for $C_{20}H_{19}N_2NaOPS_2^+$ $[M + H + Na]^+$: 421.0569, found 421.0559.

Synthesis of (5-(benzylthio)-2,2-dibutyl-1,3,4,2-thiadiazastannol-3(2*H*)-yl)diphenylphosphine oxide (Bu_2SnL). To a solution of the ligand (**H_2L**) (199.2 mg, 0.5 mmol) in methanol (10.0 mL), a solution of KOH (28.0 mg, 0.5 mmol, 1.0 equivalent) in methanol (1.0 mL) was added dropwise. The resulting mixture was stirred at room temperature for ten minutes. Subsequently, a solution of dibutyltin dichloride (151.9 mg, 0.5 mmol, 1.0 equivalent) in methanol (1.0 mL) was added dropwise to the above solution, resulting in a turbid solution.

The mixture was then refluxed for 16 h, after which it was filtered while hot. The filtrate was placed in a freezer to obtain crystals. Yield: 88.42% (278.2 mg, 0.4 mmol). ^{1}H NMR (400 MHz, DMSO-d_6) δ 7.60–7.54 (m, 4H), 7.51–7.48 (m, 2H), 7.44–7.39 (m, 4H), 7.21–7.15 (m, 5H), 4.11 (s, 2H), 1.49–1.34 (m, 8H), 1.21–1.18 (m, 4H), 0.72 (t, J = 7.3 Hz, 6H). ^{13}C NMR (101 MHz, DMSO-d_6) δ 140.24 (d, J = 29.4 Hz), 138.43, 135.22 (d, J = 115.7 Hz), 131.04, 130.94, 128.57, 128.20, 127.97 (d, J = 12.0 Hz), 126.75, 35.15, 27.41, 25.78, 25.08, 13.47. ^{31}P NMR (162 MHz, DMSO-d_6) δ 28.18. ^{119}Sn NMR (149 MHz, DMSO-d_6) δ −4.36 (d, J = 24.6 Hz). MS-ESI(m/z) calc. for $C_{28}H_{36}N_2OPS_2Sn^+$ $[M + H]^+$: 631.0123, found 631.0994. Elemental analysis: C, 53.43; H, 5.61; N, 4.45. Found: C, 53.40; H, 5.38; N, 4.42.

Synthesis of (5-(benzylthio)-2,2-diphenyl-1,3,4,2-thiadiazastannol-3(2*H*)-yl)diphenylphosphine oxide (Ph_2SnL). A solution of ligand ($\mathbf{H_2L}$) (199.2 mg, 0.5 mmol) was prepared in methanol (10.0 mL). To this, a methanolic solution of KOH (28.0 mg, 0.5 mmol, 1.0 mL) was added dropwise with continuous stirring at room temperature. After 10 minutes, a methanolic solution of diphenyl tin(IV) dichloride (206.3 mg, 0.6 mmol, 1.0 mL) was added dropwise, resulting in a turbid solution. The mixture was then refluxed for 16 h and the hot reaction mixture was filtered. The filtrate was placed in a freezer to obtain crystals. Yield: 43.28% (144.8 mg, 0.2 mmol). ^{1}H NMR (400 MHz, DMSO-d_6) δ 7.79–7.60 (m, 4H), 7.49–7.45 (m, 2H), 7.42–7.30 (m, 14H), 7.23–7.14 (m, 5H), 4.14 (s, 2H). ^{13}C NMR (101 MHz, DMSO-d_6) δ 143.65, 138.17, 135.58, 134.46 (d, J = 116.7 Hz), 131.20, 131.11, 131.06, 131.05, 129.31, 128.67, 128.26, 127.84 (d, J = 12.5 Hz), 126.84, 35.17. ^{31}P NMR (162 MHz, DMSO-d_6) δ 29.30. ^{119}Sn NMR (149 MHz, DMSO-d_6) δ −144.47 (d, J = 28.9 Hz). MS-ESI(m/z) calc. for $C_{32}H_{27}N_2NaOPS_2Sn^+$ $[M + Na]^+$: 693.0217, found 693.0215. Elemental analysis: C, 57.42; H, 4.07; N, 4.19. Found: C, 57.27; H, 3.94; N, 4.29.

X-ray crystallography

Colourless single crystals of **PL** suitable for X-ray diffraction were obtained by slow cooling of a concentrated hot solution of the compound in dichloromethane at 4.0 °C overnight. Similarly, concentrated hot methanolic solutions of compound $\mathbf{H_2L}$ and the metal complexes (Bu_2SnL and Ph_2SnL) were refrigerated overnight to afford colourless Single crystals. X-ray diffraction was performed on a Bruker D8 Venture (Photon100 CMOS detector) diffractometer, and data were collected using MoKα radiation (λ = 0.71073 Å) at room temperature. The isolated crystals were immersed in paratone oil and then mounted. The unit cell determination, data collection, data reduction, structure solution/refinement, and empirical absorption correction (SADABS) were performed using Apex III software (Bruker AXS, Madison, WI, 2015). The structure was solved by direct method and refined by the full-matrix least-squares on F^2 for all data using SHELXTL version 2017/1.63. All non-disordered non-hydrogen atoms were refined anisotropically. In the Bu_2SnL structure, the phenyl group and one of the benzenes of the phosphine oxide moieties of **L** were found to be disordered, and the refinement was performed using free variable (FVAR). We were unable to refine the solvent molecule in Ph_2SnL to a proper model and the structure was refined by excluding the electron densities from the disordered solvent molecule using PLATON/SQUEEZE,[52] which corresponds to 57 electrons per unit cell, and this can be assigned to a water molecule (≈7.5 electrons per asymmetric unit). The hydrogen atoms were placed at the calculated positions and refined using a riding model, except for the nitrogen atoms of **PL** and $\mathbf{H_2L}$, which were located on the Fourier map and refined. The crystallographic data were deposited with the Cambridge Crystallographic Data Centre, which can be obtained free of charge; the CCDC numbers are 2530292–2530295.

Powder X-ray diffraction

Bulk crystals of the compounds were obtained as described in the above section. The crystals were isolated, dried, ground in a mortar and pestle, and spread uniformly over a glass slide. All experiments were carried out on a PANalytical instrument with a Cu anode, over 2θ from 4.0 to 60.0°, and a step size of 0.02°.

Stability of complexes

The stability of the tin(IV) complexes in DMSO-d_6 and DMSO-d_6/D_2O (9 : 1, v/v) was examined using multinuclear NMR spectroscopy (^{1}H, ^{13}C, ^{31}P and ^{119}Sn). NMR spectra were recorded at 7 day intervals and analyzed to detect any changes in the spectral profile of the compound.

Lipophilicity studies (log *P* measurement)

Octanol-saturated water (OSW) and water-saturated octanol (WSO) were prepared by mixing equal volumes of octanol and saline for 24 h. A solution of each compound was prepared by adding 20.0 μL of the compound (10.0 mM in DMSO) to a mixture of 2.0 mL of WSO and 2.0 mL of OSW, then shaking the mixture. After 24 h, the sample was centrifuged at 6000 rpm for 6 minutes. The octanol and water phases were carefully separated and submitted for ICP-MS analysis. The partition coefficients of the tin(IV) complexes were calculated using the equation.

$$\log P_{o/w} = \log \frac{[C]_{WSO}}{[C]_{OSW}}.$$

Cell culture

The following cell lines, Aspc-1 (pancreatic cancer, ATCC® CCL-1682TM), HEK293T (human embryonic kidney 293T, ATCC®, CRL-3216), T-47D (breast cancer, ATCC® HTB-133TM) were obtained from American Type Culture Collection (ATCC) through LGC Promochem. Colon cancer cell line HCT116 + Chr.3 (MMR-proficient) was obtained from Baylor Scott & White Research Institute, USA. Cells were maintained in appropriate media, as recommended, with added antibiotics, penicillin/streptomycin (100 IU mL^{-1}/100.0 μg mL^{-1}, Gibco). Cells were cultured under standard conditions in T-25 or T-75 flasks (Corning® Cell Culture Flask) at 37.0 °C in a humidified incubator with 5.0% CO_2 (Forma Direct Heat CO_2 Incubator) and

 This journal is © The Royal Society of Chemistry 2026

sub-cultured when they reached 70–80% confluence. The growth medium was changed three times a week. For experimentation, sub-confluent cells were detached by trypsinization, counted in a haemocytometer and seeded on appropriate culture plates (Falcon® Culture Plate) at the indicated density. Cells were used in cellular assays after at least two passages from thawing, each with no more than 15 passages from receipt at the time of screening.

Procedure of MTT assay

Cells were seeded in 96-well plates at a density of 5×10^3 cells per well, followed by an incubation at 37.0 °C with 5.0% CO_2 for 24 h. The stock solutions of the compounds were prepared by dissolving in DMSO to obtain a concentration of 10.0 mM. The cells were treated with increasing concentrations of the compounds diluted in cell media, achieving a total volume of 200 μL. The cells were incubated for an additional 48 h, and then the media were replaced with fresh media (100 μL), and 10.0 μL of MTT (3-(4,5-dimethyl-2-thiazolyl)-2,5-diphenyl-2*H*-tetrazolium bromide) (5.0 mg mL^{-1}) was added to each well. After 4 h of incubation, the cell media was removed, and formazan crystals were dissolved in dimethyl sulfoxide (100 μL per well). The absorbance at 570 nm in each well was determined using an EMax Plus microplate reader (Thermo Scientific). Cell viability of each well was determined by subtracting the average absorbance of the blank group. Cell viability was calculated using the equation as below:

$$\text{Cell viability}\,(\%) = \frac{(A_{\text{sample}} - A_{\text{blank}})}{(A_{\text{control}} - A_{\text{blank}})} \times 100$$

where A_{sample}, A_{control} and A_{blank} represent the absorption of cells containing sample, no sample, and neither sample, nor cells, respectively. IC_{50} values were calculated using GraphPad Prism software. *XY* analysis with three replicate values in side-by-side sub-columns was chosen. *X* values were transformed to logarithms; data were normalized. Data were then analysed with *XY* analysis "Nonlinear regression (curve fit)" and "log (inhibitor) *vs.* normalized response".

Whole cell uptake studies

The T-47D cells were incubated with the compound (1.0 μM) for 24 h at 37.0 °C. After this time, the cells were washed with PBS. The cells were detached with trypsin, harvested, centrifuged, and resuspended. The number of cells on each dish was accurately counted. Each sample was digested using a 10% HCl solution. The tin (Sn) content was determined by ICP-MS and compared with tin reference standards. The tin-metal content was then associated with the number of cells.

Intracellular distribution by ICP-MS

The subcellular-localization of the tin(IV) complexes was determined by measuring tin-metal content within the T-47D cell using ICP-MS. 4.0×10^6 cells were incubated with the compound (1.0 μM) for 24 h at 37.0 °C. After this time, the cells were detached with trypsin, harvested, and the cell count was accurately determined. The amount was divided equally into two portions. In the first portion, the nucleus was extracted using a nucleus extraction kit (abcam); in the second portion, the mitochondria were extracted using a mitochondria extraction kit (abcam). Each sample was digested using a 10.0% HCl solution. The tin content was determined using an ICP-MS apparatus and compared with the Sn reference standard. The tin content was then associated with the number of cells. The reported % values represent the fraction of tin measured in the nucleus and mitochondria relative to the total cellular uptake.

Cell cycle analysis

In brief, T-47D breast cancer cells (1.0×10^6) were seeded in 6-well plates with 2.0 mL of media per well and incubated for 24 h. After incubation, the supernatant was removed, and the cells were treated with 0.3 μM of the compounds for 24 h. After the treatment, the supernatant was discarded, and the cells were washed with PBS. Cell pellets were obtained using trypsinization, collected by centrifugation, and washed again with PBS. The pellets were then resuspended in ice-cold 70.0% ethanol and stored at −20.0 °C for 4 h for fixation. After removing ethanol, cells were washed with PBS and resuspended in 300 μL of FxCycle™ PI/RNase Staining Solution for 30 minutes in the dark at room temperature. Samples were analysed in triplicate by flow cytometry using an Attune™ NxT Acoustic Focusing Cytometer, with propidium iodide (PI) detected in the YL2 channel. The data were processed using a Watson (Pragmatic) fitting algorithm in FlowJo.

Apoptosis analysis

T-47D cells were seeded into a 6-well plate at a density of approximately 1.0×10^5 cells per well and then incubated for 24 h in 2.0 mL of medium. Afterward, the medium was removed and replaced with fresh medium containing tin(IV) complex or cisplatin (5.0 μM). The cells were incubated for an additional 4 h. The media were then removed, and the cells were washed with 2.0 mL of PBS. Cells were trypsinized (0.5 mL), followed by the addition of 2.0 mL DMEM per well. Cell suspensions were centrifuged to form a pellet and was washed with PBS. Cells were resuspended in 200 μL binding buffer (1×) at a density of 5.0×10^5 cells per mL, and 5.0 μL Annexin V-FITC was added to 195 μL of the cell suspension. The mixture was incubated for 10 minutes at room temperature, washed with 200 μL binding buffer (1×), and resuspended in 190 μL binding buffer (1×). Then, 10.0 μL of propidium iodide (20.0 μg mL^{-1}) was added, and apoptosis analysis was performed by flow cytometry using an Attune™ NxT Acoustic Focusing Cytometer, with Annexin V-FITC and propidium iodide (PI) detected in the BL1 and YL2 channel, respectively. The data was analysed using FlowJo.

Cellular ATP depletion assay

The intracellular ATP level was measured utilizing the Luminescent ATP Detection Assay Kit (Abcam, ab113849). T-47D cells were seeded in a white 96-well plate and incubated

for 24 h. The cells were then treated with Bu_2SnL, Ph_2SnL, and cisplatin at concentrations equivalent to the IC_{50} and $2 \times IC_{50}$ values for each compound. After 24 h treatment, the culture medium was removed, and cells were washed three times with cold phosphate-buffered saline (PBS). Subsequently, 50.0 μL of detergent was added to each well. The plate was sealed and agitated in an orbital shaker at 600–700 rpm for 5 minutes to lyse the cells and stabilize the ATP. Afterward, 50.0 μL of substrate solution was dispensed into each well, and the plate was again sealed and shaken for 5 minutes at 600–700 rpm. The plate was then dark-adapted by covering for 10 minutes before luminescence measurement. Luminescence intensities were normalized relative to the untreated control.

Reactive oxygen species (ROS) generation study

T-47D cells were seeded into a 6-well plate at a density of approximately 1×10^5 cells per well, followed by incubation for 24 h in 2.0 mL of medium. Afterward, the medium was removed and replaced with fresh medium containing tin(IV) complexes (5.0 μM). The cells were incubated for an additional 4 h. The media were removed, and the cells were washed with 2.0 mL of PBS, then incubated with 10.0 μM DCFH-DA for 30 minutes. The media were then removed, and the cells were washed with 2.0 mL of PBS. Cells were trypsinized (0.5 mL), followed by the addition of 2.0 mL DMEM per well. Cells suspensions were centrifuged to form a pellet and washed with PBS. Cells were resuspended in 500 μL PBS. The ROS analysis was performed using a BD FACSymphony flow cytometer (BD Bioscience) within an hour of sample preparation.

DAPI displacement assay

Solutions of ctDNA were prepared by dissolving ctDNA in Tris-HCl/NaCl buffer at pH = 7.4 (50.0 mM NaCl/5.0 mM Tris-HCl). A solution of ctDNA in the buffer showed a UV absorbance ratio of about 1.9 at 260.0 and 280.0 nm, indicating that the DNA was sufficiently free of protein. The DNA concentration per nucleotide was determined by absorption spectroscopy using the molar extinction coefficient value of 6600.0 M^{-1} cm^{-1} at 260.0 nm. The ctDNA solution was diluted several times with the buffer to achieve the desired concentration. Stock solution of DAPI-bound ctDNA ([DAPI] = 1.0 μM and [ctDNA] = 5.0 μM) was stored at 4.0 °C and used within 4 days. Aliquots of the Bu_2SnL were added to a 3.0 mL solution of DAPI-bound ctDNA (5.0 mM Tris-HCl, 50.0 mM NaCl, pH = 7.4 at 25 °C). And the mixtures were allowed to stand for 15 minutes before fluorescence measurements.

EB displacement assay

The ctDNA solutions were prepared by dissolving ctDNA in Tris-HCl/NaCl buffer at pH = 7.4 (50.0 mM NaCl/5 mM Tris-HCl). A solution of ctDNA in the buffer displayed a UV absorbance ratio of about 1.9 at 260.0 and 280.0 nm, indicating that the DNA was sufficiently free of protein. The DNA concentration per nucleotide was determined by absorption spectroscopy using a molar extinction coefficient of 6600 M^{-1} cm^{-1} at 260.0 nm. The ctDNA solution was diluted several times with the buffer to the desired concentration. Stock solution of EB-bound ctDNA ([EB] = 4.0 μM and [ctDNA] = 28.0 μM) was stored at 4.0 °C and used within 4 days. Aliquots of the Bu_2SnL were added to a 3.0 mL solution of EB-bound ctDNA (5.0 mM Tris-HCl, 50.0 mM NaCl, pH = 7.4 at 25.0 °C). And the mixtures were allowed to stand for 15 minutes before fluorescence measurements.

Mechanism of action

A solution of diethylphosphite (12.8 μL, 0.1 mmol) in 5.0 mL of ethanol was prepared and stirred at room temperature. To this solution, one equivalent of potassium hydroxide (KOH) was added, and the mixture was stirred for 10 minutes to yield potassium ethyl phosphonate. Subsequently, one equivalent of Bu_2SnL (62.9 mg, 0.1 mmol) was added, and the reaction mixture was heated to 70.0 °C with stirring for an hour. After completion of the reaction, the mixture was filtered to remove any insoluble material. The resulting filtrate was analysed by electrospray ionization mass spectrometry (ESI-MS) to confirm the formation of the coordination complex. Approximately 20.0 mg of metal complex (Bu_2SnL, Ph_2SnL, Bu_2SnCl_2 or Ph_2SnCl_2) was dissolved in 500 μL DMSO-d_6 and transferred into an NMR tube, and ^{31}P and ^{119}Sn NMR spectra were recorded to characterise the free complex. Subsequently, 0.1–5.0 equivalents of phosphonate or guanosine monophosphate triethyl ammonium salt (5.0 eq. dissolved in 100.0 μL DMSO-d_6) were added directly to the NMR tube, and the mixture was gently mixed to ensure homogeneity. Similarly, 0.1–1.0 equivalents of 2′-deoxyguanosine monohydrate or diethyl phosphite (1.0 equivalent dissolved in 100.0 μL DMSO-d_6) were added directly to the NMR tube of Bu_2SnL. The ^{31}P and ^{119}Sn NMR spectra were then recorded to monitor any changes in chemical shifts.

Comet assay

The T-47D cells were seeded into 6-well plates (0.1 million each) and incubated for 24 h. Cells were then treated with Bu_2SnL (5.0 μM) for 2 h and 4 h. After treatment, cells were gently detached from the wells using a rubber policeman, collected into conical tubes, and centrifuged at a speed of 700*g* for two minutes. The supernatant was discarded, and the cell pellet was washed once with ice-cold PBS devoid of Mg^{2+} and Ca^{2+}. Following centrifugation and removal of the supernatant liquid, the cells were resuspended in an ice-cold PBS (devoid of Mg^{2+} and Ca^{2+}) at a density of 1×10^5 cells per mL. Cell suspensions were combined with comet agarose at a 1 : 9 (v/v) ratio and spread onto the slides precoated with comet agarose. Slides were maintained horizontally, transferred to the dark, and kept at 4.0 °C for 15 minutes to allow solidification. The slides were then immersed in pre-chilled Lysis Buffer (approximately 25.0 mL per slide) for 60 minutes at 4.0 °C in the dark. The lysis buffer was then gently aspirated and replaced with pre-chilled alkaline solution (approximately 25.0 mL per slide), and the slides were incubated for a further 30 minutes at 4.0 °C in the dark. Following equilibration in pre-chilled alkaline electrophoresis buffer, the slides were subjected to electro-

 This journal is © The Royal Society of Chemistry 2026

phoresis at 25.0 V and 300.0 mA for 25 minutes. After electrophoresis, the slides were washed twice with ice-cold deionized water, immersed in ice-cold 70% ethanol for five minutes, and air-dried for 30 minutes. Later, the slides were stained with Vista Green DNA Dye for 15 minutes and analysed with epifluorescence microscopy using a FITC filter.

Author contributions

Conceptualization, S. S. and K. K. D.; methodology, S. S., H. M. O, M. H. O. and K. K. D.; data curation, S. S.; investigation, S. S. H. M. O., M. H. O., S. T. H. and K. K. D.; writing—original draft, S. S. and K. K. D.; writing—review & editing, S. S. H. M. O., M. H. O., S. T. H. and K. K. D.; funding acquisition, K. K. D.; resources, M. H. O. and K. K. D.; supervision, H. M. O., M. H. O. and K. K. D.

Conflicts of interest

The authors declare the following competing financial interest (s): Authors, S. Sharma, M. H. Ögmundsdóttir, H. M. Ögmundsdóttir, and K. K. Damodaran are inventors on a pending patent application filed by University of Iceland, which is related to the compounds and their anticancer activity described in this manuscript.

Data availability

All data needed to support the conclusions of this manuscript are included in the main text and the supplementary information (SI). Supplementary information: synthetic details, NMR spectra (^{1}H, ^{13}C, ^{31}P, and ^{119}Sn), IR, and ESI-MS of compounds, CIF files of compounds, aqueous stability using NMR, crystallographic details, ROS generation, MTT cell viability plots in various cell lines, log($P_{o/w}$) values, flow cytometry images of apoptosis and cell cycle analysis. See DOI: https://doi.org/10.1039/d6dt00812g.

CCDC 2530292–2530295 contain the supplementary crystallographic data for this paper.[70a–d]

Acknowledgements

We are grateful to the University of Iceland Research Fund, Icelandic cancer society (Krabbameinsfélag Íslands), and Icelandic Research Fund, Rannís Iceland (IRF-2511569-051) for providing financial support. SS thankfully acknowledge Rannís Iceland (IRF-2410559-052) for the doctoral grant. We thank Gunnar Widtefeldt Reginsson and Sigrídur Jónsdóttir, Universi-ty of Iceland, for NMR and mass spectrometry. We thank Johann Gunnarsson Robin, University of Iceland, for his kind assistance with the ICP-MS experiments.

References

1 F. Bray, M. Laversanne, H. Sung, J. Ferlay, R. L. Siegel, I. Soerjomataram and A. Jemal, *CA Cancer J. Clin.*, 2024, **74**, 229–263.
2 K. Bukowski, M. Kciuk and R. Kontek, *Int. J. Mol. Sci.*, 2020, **21**, 3233.
3 U. Ndagi, N. Mhlongo and M. E. Soliman, *Drug Des., Dev. Ther.*, 2017, **11**, 599–616.
4 E. Wiltshaw, *Platinum Met. Rev.*, 1979, **23**, 90–98.
5 S. Dilruba and G. V. Kalayda, *Cancer Chemother. Pharmacol.*, 2016, **77**, 1103–1124.
6 P. M. Bruno, Y. Liu, G. Y. Park, J. Murai, C. E. Koch, T. J. Eisen, J. R. Pritchard, Y. Pommier, S. J. Lippard and M. T. Hemann, *Nat. Med.*, 2017, **23**, 461–471.
7 K. Peng, Y. Zheng, W. Xia and Z.-W. Mao, *Chem. Soc. Rev.*, 2023, **52**, 2790–2832.
8 C. Li, L. Tu, Y. Xu, M. Li, J. Du, P. J. Stang, Y. Sun and Y. Sun, *Angew. Chem., Int. Ed.*, 2024, **63**, e202406392.
9 S. Rottenberg, C. Disler and P. Perego, *Nat. Rev. Cancer*, 2021, **21**, 37–50.
10 R. A. Ward, S. Fawell, N. Floc'h, V. Flemington, D. McKerrecher and P. D. Smith, *Chem. Rev.*, 2021, **121**, 3297–3351.
11 R. G. Kenny and C. J. Marmion, *Chem. Rev.*, 2019, **119**, 1058–1137.
12 K. Xiong, C. Ouyang, J. Liu, J. Karges, X. Lin, X. Chen, Y. Chen, J. Wan, L. Ji and H. Chao, *Angew. Chem., Int. Ed.*, 2022, **61**, e202204866.
13 A. R. Rubio, R. González, N. Busto, M. Vaquero, A. L. Iglesias, F. A. Jalón, G. Espino, A. M. Rodríguez, B. García and B. R. Manzano, *Pharmaceutics*, 2021, **13**, 1540.
14 M. G. Ferraro, M. Piccolo, G. Misso, R. Santamaria and C. Irace, *Pharmaceutics*, 2022, **14**, 954.
15 I. Amarsy, S. Papot and G. Gasser, *Angew. Chem., Int. Ed.*, 2022, **61**, e202205900.
16 S. Thota, D. A. Rodrigues, D. C. Crans and E. J. Barreiro, *J. Med. Chem.*, 2018, **61**, 5805–5821.
17 C. S. Allardyce and P. J. Dyson, *Dalton Trans.*, 2016, **45**, 3201–3209.
18 F. H. Abdalbari and C. M. Telleria, *Discover Oncol.*, 2021, **12**, 42.
19 S. N. Syed Annuar, N. F. Kamaludin, N. Awang and K. M. Chan, *Front. Chem.*, 2021, **9**, 657599.
20 N. A. Abd Aziz, N. Awang, K. M. Chan, N. F. Kamaludin and N. N. Mohamad Anuar, *Molecules*, 2023, **28**, 5841.
21 R. Joshi, N. Tomar, S. Pokharia and I. Joshi, *Results Chem.*, 2023, **5**, 100955.
22 S. Sharma, V. Kaur, P. Duhan, R. Singh and N. Agnihotri, *J. Med. Chem.*, 2025, **68**, 2593–2607.
23 J. C. Lima and L. Rodriguez, *Adv. Anticancer Agents Med. Chem.*, 2011, **11**, 921–928.
24 D. Jai and Y. Jyoti, *Adv. Anticancer Agents Med. Chem.*, 2018, **18**, 335–353.
25 S. Ali, S. Shahzadi and Imtiaz-ud-Din, *Iran. J. Sci. Technol., Trans. A: Sci.*, 2018, **42**, 505–524.

26 A. Khan, S. Parveen, A. Khalid and S. Shafi, *Inorg. Chim. Acta*, 2020, **505**, 119464.
27 A. K. Saxena and F. Huber, *Coord. Chem. Rev.*, 1989, **95**, 109–123.
28 M. Balogová, S. Sharma, P. Cherek, S. N. Ólafsson, S. Jónsdóttir, H. M. Ögmundsdóttir and K. K. Damodaran, *Dalton Trans.*, 2022, **51**, 13119–13128.
29 J. Sheng, J. Gan and Z. Huang, *Med. Res. Rev.*, 2013, **33**, 1119–1173.
30 J. Qian, G. Liao, M. Chen, R.-W. Peng, X. Yan, J. Du, R. Huang, M. Pan, Y. Lin, X. Gong, G. Xu, B. Zheng, C. Chen and Z. Yang, *Front. Pharmacol.*, 2024, **15**, 1474337.
31 T. Makovec, *Radiol. Oncol.*, 2019, **53**, 148–158.
32 S. Komeda, T. Moulaei, K. K. Woods, M. Chikuma, N. P. Farrell and L. D. Williams, *J. Am. Chem. Soc.*, 2006, **128**, 16092–16103.
33 P. Yang and M. Guo, *Coord. Chem. Rev.*, 1999, **185–186**, 189–211.
34 G. Gasser, I. Ott and N. Metzler-Nolte, *J. Med. Chem.*, 2011, **54**, 3–25.
35 R. Castro-Ramírez and N. Barba-Behrens, *Dalton Trans.*, 2025, **54**, 15964–15979.
36 C. M. C. Andrés, J. M. Pérez de la Lastra, E. Bustamante Munguira, C. Andrés Juan and E. Pérez-Lebeña, *Int. J. Mol. Sci.*, 2024, **25**, 7314.
37 N. Gerasimchuk, T. Maher, P. Durham, K. V. Domasevitch, J. Wilking and A. Mokhir, *Inorg. Chem.*, 2007, **46**, 7268–7284.
38 M. Hanif, J. Arshad, J. W. Astin, Z. Rana, A. Zafar, S. Movassaghi, E. Leung, K. Patel, T. Söhnel, J. Reynisson, V. Sarojini, R. J. Rosengren, S. M. F. Jamieson and C. G. Hartinger, *Angew. Chem., Int. Ed.*, 2020, **59**, 14609–14614.
39 J. B. Rodriguez and C. Gallo-Rodriguez, *ChemMedChem*, 2019, **14**, 190–216.
40 B. R. Smith, C. M. Eastman and J. T. Njardarson, *J. Med. Chem.*, 2014, **57**, 9764–9773.
41 M. King, S. Joseph, A. Albert, T. V. Thomas, M. R. Nittala, W. C. Woods, S. Vijayakumar and S. Packianathan, *Oncology*, 2019, **98**, 61–80.
42 K. L. Dechant, R. N. Brogden, T. Pilkington and D. Faulds, *Drugs*, 1991, **42**, 428–467.
43 X. Huang, Y. Hou, X. Weng, W. Pang, L. Hou, Y. Liang, Y. Wang, L. Du, T. Wu, M. Yao, J. Wang and X. Meng, *Oncogenesis*, 2021, **10**, 4.
44 M. Karsa, L. Xiao, E. Ronca, A. Bongers, D. Spurling, A. Karsa, S. Cantilena, A. Mariana, T. W. Failes, G. M. Arndt, L. C. Cheung, R. S. Kotecha, R. Sutton, R. B. Lock, O. Williams, J. de Boer, M. Haber, M. D. Norris, M. J. Henderson and K. Somers, *J. Mol. Med.*, 2024, **102**, 507–519.
45 C. L. Loprinzi, R. M. Goldberg, J. Q. Su, J. A. Mailliard, S. A. Kuross, A. W. Maksymiuk, J. W. Kugler, J. R. Jett, C. Ghosh and D. M. Pfeifle, *J. Clin. Oncol.*, 1994, **12**, 1126–1129.
46 R. T. Chlebowski, L. Bulcavage, M. Grosvenor, R. Tsunokai, J. B. Block, D. Heber, M. Scrooc, J. S. Chlebowski, J. Chi, E. Oktay, S. Akman and I. Ali, *Cancer*, 1987, **59**, 406–410.
47 U. Anthoni, B. M. Dahl, C. Larsen, P. H. Nielsen, A. A. Lindberg, G. Jansen, B. Lamm and B. Samuelsson, *Acta Chem. Scand.*, 1969, **23**, 1061–1063.
48 F. N. F. How, K. A. Crouse, M. I. M. Tahir, M. T. H. Tarafder and A. R. Cowley, *Polyhedron*, 2008, **27**, 3325–3329.
49 U. Sair and A. Thakur, *Mater. Today: Proc.*, 2022, **50**, 1862–1866.
50 J. Devi, J. Yadav, D. Kumar, D. K. Jindal and B. Basu, *Appl. Organomet. Chem.*, 2020, **34**, e5815.
51 G. F. de Sousa, J. R. Sabino, I. Vencato, C. A. L. Filgueiras and J. D. Ardisson, *J. Braz. Chem. Soc.*, 2009, **20**, 1425–1433.
52 G. Sheldrick, *Acta Crystallogr., Sect. C: Cryst. Struct. Commun.*, 2015, **71**, 3–8.
53 B. Kristinsson, M. Janiw and K. K. Damodaran, *ChemPlusChem*, 2024, **89**, e202400351.
54 A. Levina, D. C. Crans and P. A. Lay, *Coord. Chem. Rev.*, 2017, **352**, 473–498.
55 J. van Meerloo, G. J. L. Kaspers and J. Cloos, in *Cancer Cell Culture: Methods and Protocols*, ed. I. A. Cree, Humana Press, Totowa, NJ, 2011, pp. 237–245.
56 J. A. Arnott and S. L. Planey, *Expert Opin. Drug Discovery*, 2012, **7**, 863–875.
57 H. Ullah, V. Previtali, H. B. Mihigo, B. Twamley, M. K. Rauf, F. Javed, A. Waseem, R. J. Baker and I. Rozas, *Eur. J. Med. Chem.*, 2019, **181**, 111544.
58 K. Choroba, B. Zowiślok, S. Kula, B. Machura, A. M. Maroń, K. Erfurt, C. Marques, S. Cordeiro, P. V. Baptista and A. R. Fernandes, *J. Med. Chem.*, 2024, **67**, 19475–19502.
59 C. Nössing and K. M. Ryan, *Br. J. Cancer*, 2023, **128**, 426–431.
60 A. T. Dharmaraja, *J. Med. Chem.*, 2017, **60**, 3221–3240.
61 B. Kar, A. Rahaman, M. Pal, A. Banerjee, M. Roy, R. Chakrabarty, S. Bhattacharjee, D. P. Mandal and P. Paira, *J. Med. Chem.*, 2025, **68**, 20011–20036.
62 A. Jug and J. Ilaš, *RSC Med. Chem.*, 2025, **16**, 4044–4067.
63 C. Gonzalo-Navarro, E. Zafon, J. A. Organero, F. A. Jalón, J. C. Lima, G. Espino, A. M. Rodríguez, L. Santos, A. J. Moro, S. Barrabés, J. Castro, J. Camacho-Aguayo, A. Massaguer, B. R. Manzano and G. Durá, *J. Med. Chem.*, 2024, **67**, 1783–1811.
64 D. Romani, F. Marchetti, C. Di Nicola, M. Cuccioloni, C. Gong, A. M. Eleuteri, A. Galindo, F. Fadaei-Tirani, M. Nabissi and R. Pettinari, *J. Med. Chem.*, 2023, **66**, 3212–3225.
65 K. L. Haas and K. J. Franz, *Chem. Rev.*, 2009, **109**, 4921–4960.
66 M. Pooyan, Z. Shariatinia, F. Mohammadpanah, K. Gholivand, M. Dusek, V. Eigner, M. Satari and A. A. E. Valmoozi, *J. Mol. Liq.*, 2023, **391**, 123442.
67 A. Paul, R. A. Khan, G. M. Shaik, J. P. Shaik, D. S. Nesterov, M. F. C. Guedes da Silva and A. J. L. Pombeiro, *New J. Chem.*, 2024, **48**, 2907–2919.

 This journal is © The Royal Society of Chemistry 2026

68 J. Holeček, M. Nádvorník, K. Handlíř and A. Lyčka, *J. Organomet. Chem.*, 1986, **315**, 299–308.
69 V. B. Pathi, S. Kumar, A. Sk, S. Shee, M. K. Ghosh and B. Banerji, *J. Med. Chem.*, 2025, **68**, 19153–19168.
70 (*a*) CCDC 2530292: Experimental Crystal Structure Determination, 2026, DOI: 10.5517/ccdc.csd.cc2qxzbz; (*b*) CCDC 2530293: Experimental Crystal Structure Determination, 2026, DOI: 10.5517/ccdc.csd.cc2qxzc0; (*c*) CCDC 2530294: Experimental Crystal Structure Determination, 2026, DOI: 10.5517/ccdc.csd.cc2qxzd1; (*d*) CCDC 2530295: Experimental Crystal Structure Determination, 2026, DOI: 10.5517/ccdc.csd.cc2qxzf2.